The Solution Structure and Dynamics of an Arc Repressor Mutant Reveal Premelting Conformational Changes Related to DNA Binding†

Irene M. A. Nooren,‡ Alex W. M. Rietveld,‡,§ Giuseppe Melacini,‡ Robert T. Sauer,|| Robert Kaptein,‡ and Rolf Boelens*,‡

Department of NMR Spectroscopy, Bijvoet Center for Biomolecular Research, Utrecht University, Padualaan 8, 3584 CH Utrecht, The Netherlands, and Department of Biology, Massachusetts Institute of Technology, Cambridge, Massachusetts 02139

Received November 10, 1998; Revised Manuscript Received February 1, 1999

ABSTRACT: The solution structure of the hyperstable MYL mutant (R31M/E36Y/R40L) of the Arc repressor of bacteriophage P22 was determined by NMR spectroscopy and compared to that of the wild-type Arc repressor. A backbone rmsd versus the average of 0.37 Å was obtained for the well-defined core region. For both Arc-MYL and the wild-type Arc repressor, evidence for a fast equilibrium between a packed ("in") conformation and an extended ("out") conformation of the side chain of Phe 10 was found. In the MYL mutant, the "out" conformation is more highly populated than in the wild-type Arc repressor. The Phe 10 is situated in the DNA-binding β-sheet of the Arc dimer. While its "in" conformation appears to be the most stable, the "out" conformation is known to be present in the operator-bound form of Arc, where the Phe 10 ring contacts the phosphate backbone [Raumann, B. E., et al. (1994) *Nature 367*, 754−757]. As well as DNA binding, denaturation by urea and high temperatures induces the functionally active "out" conformation. With a repacking of the hydrophobic core, this characterizes a premelting transition of the Arc repressor. The dynamical properties of the Arc-MYL and the wild-type Arc repressor were further characterized by ^{15}N relaxation and hydrogen−deuterium exchange experiments. The increased main chain mobility at the DNA binding site compared to that of the core of the protein as well as the reorientation of the side chain of Phe 10 is suggested to play an important role in specific DNA binding.

When DNA binding proteins bind to their target, structural alterations in the DNA binding site can often be identified. This is commonly referred to as an "induced fit" binding mechanism. This study describes the dynamical processes in the DNA binding site of the dimeric Arc repressor of *Salmonella* bacteriophage P22 that provide insight into this induced fit mechanism. Together with the Mnt repressor, the Arc repressor is involved in the switch between the lysogenic and lytic pathways of the phage by regulating the transcription of the *ant* gene during lytic growth (*1, 2*). Both the structures of the free Arc repressor (*3*) and the protein in complex with its operator (*4*) have been determined. The solution structure of the free Arc dimer shows that the two 53-residue peptide chains of Arc are highly intertwined, forming an intermonomeric antiparallel β-sheet (residues 8−14) and closely packed α-helices (residues 16−29 and 34−46). In the complex with DNA, two Arc dimers are bound to its partially symmetric 21 bp operator, where each dimer uses the antiparallel β-sheet to bind into the successive major grooves of the DNA.

Several structural rearrangements in the DNA-binding site of the Arc dimer occur upon operator binding (*4, 5*). First, the N-terminal region (residues 1−7), which is disordered in the free protein, becomes structured in the DNA complex, thereby interacting with the DNA backbone phosphates. Second, a significant structural difference between the free and DNA-bound forms of the Arc repressor is observed in the conformation of the side chain of Phe 10. In the unbound Arc dimer, the Phe 10 side chain is part of the hydrophobic core (Figure 1a), whereas upon DNA binding, this side chain swings out to pack against the phosphate oxygens of the DNA backbone (Figure 1b). Mutagenesis studies showed that substitution of the phenylalanine by a valine does not affect the stability of the protein but leads to a 120-fold reduction in DNA binding specificity with a reduction in the aspecific affinity of only a factor of 2 (*6*). The neighboring residues Gln 9, Asn 11, and Arg 13 are also known to be involved in recognition, establishing specific contacts with the DNA bases (*7*). The precise role of Phe 10 in recognition is less clear however.

A close comparison of all currently known unbound Arc wild-type (Arc-wt) and mutant structures reveals conformational differences in the DNA binding site, similar to those that occur upon DNA binding. As shown in Figure 1c, two distinct conformations exist, which mainly differ in the rotameric state of the χ_1 dihedral angle of Phe 10 and which also involve structural adjustments in the backbone torsion angles of residues 9−11. In both the NMR and crystal structure of Arc-wt (C. Kissinger, U. Obeysekare, L. Keefe,

† This work was supported by the Life Sciences Foundation of the Netherlands Organization for Scientific Research (NWO) (Project 805-02.072).

* To whom correspondence should be addressed. Phone: +31-30-2534035. Fax: +31-30-2537623. E-mail: boelens@nmr.chem.uu.nl.

‡ Utrecht University.

§ Present address: Departamento de Bioquímica Médica, Universidade Federal do Rio de Janeiro, Rio de Janeiro RJ 21941-590, Brazil.

|| Massachusetts Institute of Technology.

10.1021/bi982677t CCC: $18.00
Published on Web 04/24/1999

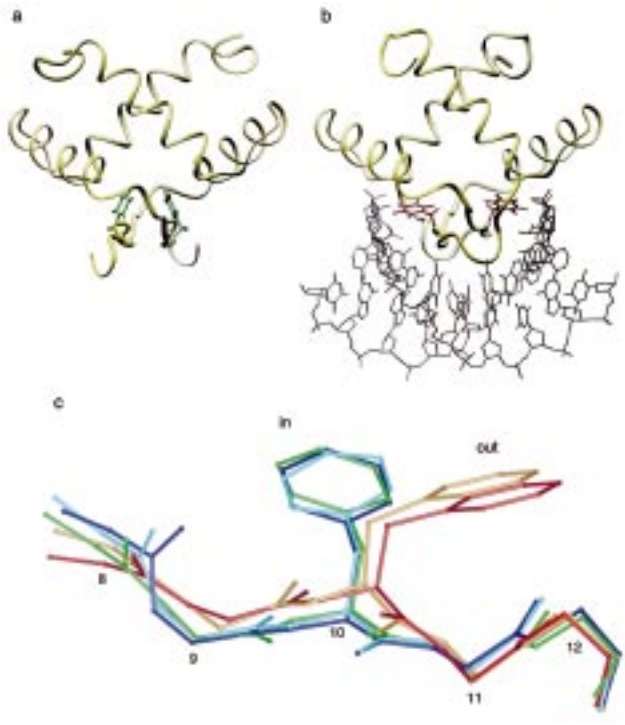

FIGURE 1: Representation of the conformation of the side chain of Phe 10 in the NMR structure of the free Arc-wt protein (a) and in the X-ray structure of the Arc-wt−DNA complex (b). The protein backbone is shown as a ribbon, and the nucleic acid and Phe 10 side chains are shown as a ball-and-stick representations. (c) Best-fit superposition of the backbone atoms (residues 8−14) of all known Arc structures, displaying the backbone position of residues 8−12 and the Phe 10 side chain conformation of one monomeric unit: the NMR structure of Arc-wt (green), the crystal structure of Arc-wt (light blue), the crystal structure of Arc PL8 (violet), the crystal structure of Arc-MYL (yellow), and the crystal structure of Arc-wt in complex with DNA (red). Only heavy atoms are displayed; the positions of the Cα atoms are denoted.

B. Raumann, R. Sauer, and C. Pabo, unpublished results) and the crystal structure of the hyperstable Arc-PL8 mutant (*8*), the aromatic ring is packed in the core of the protein with a gauche$^-$ rotameric state ($\chi_1 \sim 60°$), while in the hyperstable Arc-MYL mutant (R31M/E36Y/R40L) (*9*), Phe 10 adopts the trans conformation ($\chi_1 \sim 180°$) similar to that in the cocrystal structure of Arc (Figure 1c). We refer to these two conformations as the "in" and "out" conformations, respectively.

Previous NMR studies with the wild-type Arc repressor showed a strong temperature dependence of the chemical shifts of the aromatic protons of Phe 10 in a temperature range that is below the point at which the wild-type Arc repressor begins to denaturate, i.e., at approximately 50 °C (*10*−*12*). Optical studies of denaturant-induced unfolding suggested a native-like dimeric folding intermediate of the Arc repressor (*13*, *14*). These findings strongly imply the existence of a premelting conformational transition and led us to use NMR to further investigate structural alterations in the DNA binding region of the Arc repressor based on the structure of the MYL mutant in solution under different denaturating conditions. The Arc-MYL mutant allows the use of a wide range of temperatures due to its increased stability, which is established by replacing the wild-type intramonomeric salt bridge and hydrogen-bonded network in the core of the protein by hydrophobic packing (*9*). The solution structure of the Arc-MYL mutant was determined, and the conformations that were accessible for the Phe 10 side chain were characterized by chemical shift, NOE,[1] and *J* coupling data obtained at different temperatures. Both the MYL mutant and Arc-wt repressor display a fast equilibrium between the "in" and "out" conformations of Phe 10. However, the population of the "out" conformation was found to be significantly higher for the MYL mutant. The "out" conformation of Phe 10 that is induced by DNA binding can be induced both by high temperatures and by urea. Thus, the main features of the premelting of the Arc repressor involve the reorientation of the aromatic ring of Phe 10 and reorganization of neighboring core residues. The structural studies reveal a dynamic character of the β-sheet region in the Arc repressor, an observation that is supported by ^{15}N relaxation and hydrogen−deuterium exchange data.

MATERIALS AND METHODS

Sample Preparation. Uniformly ^{15}N-labeled Arc-wt and Arc-MYL were isolated from *Escherichia coli* strain X90 containing plasmids pTA200 and pSA300, respectively, as described previously (*2*). The ^{15}N isotope was incorporated by growing the cells on a minimal medium using 0.5 g/L $^{15}NH_4Cl$ and 10 g/L glucose. The protein was dissolved in 95% H_2O/5% D_2O (v/v) containing 50 mM KP_i and 150 mM NaCl and buffered at pH 4.5. To avoid bacterial growth in the sample, 0.01% azide was added. Protein concentrations of the various NMR samples were between 0.5 and 2.6 mM, as measured by UV absorption.

NMR Measurements. NMR experiments were performed at 500 or 600 MHz on Bruker AMX spectrometers at 30 °C, unless otherwise indicated. The TOCSY experiments were carried out using a clean-MLEV17 sequence (*15*) with mixing times ranging from 30 to 90 ms and NOESY spectra (*16*) with NOE mixing times ranging from 75 to 175 ms. In addition, three-dimensional (3D) gradient-enhanced NOESY-(^{1}H,^{15}N)-HSQC and TOCSY-(^{1}H,^{15}N)-HSQC spectra with mixing times of 100 and 60 ms, respectively, were recorded. For the determination of the χ_1 rotameric state of Phe 10, NOESY, TOCSY, and ROESY (*17*) experiments with short mixing times were also carried out. The one-dimensional (1D) and two-dimensional (2D) spectra at different temperatures were calibrated on the HDO signal according to the method of Cavanagh et al. (*18*). For the urea titration experiments, 1D spectra were calibrated on the urea NH_2 signal.

{^{1}H}−^{15}N heteronuclear NOE relaxation experiments were recorded at 600 MHz and 30 °C as described previously (*19*, *20*). The hydrogen−deuterium exchange rates were measured by dissolving the lyophilized protonated protein in D_2O and recording a series of short (^{1}H,^{15}N)-HSQC spectra. Triton, NMRPipe (*21*), and Biosym Felix (Molecular Simulations Inc.) software packages were used for NMR data processing, and the Regine package was used for spectral bookkeeping and distance restraints collection. Software developed in-house was used to analyze the relaxation and H−D exchange data (*20*). The {^{1}H}−^{15}N heteronuclear NOE data are given

[1] Abbreviations: 2D, two-dimensional; 3D, three-dimensional; NOE, nuclear Overhauser effect; NOESY, NOE spectroscopy; TOCSY, total correlated spectroscopy; HSQC, heteronuclear single-quantum coherence; rmsd, root-mean-square deviation.

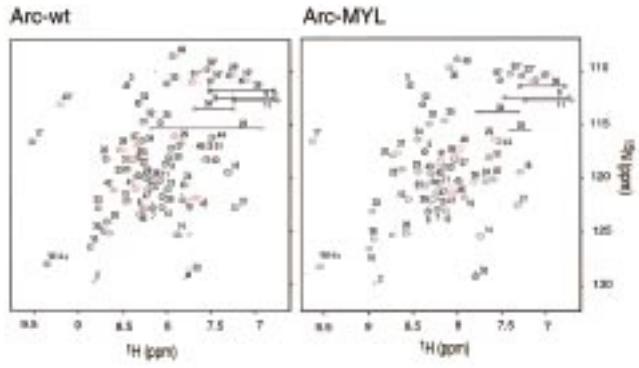

FIGURE 2: (^{1}H,^{15}N)-HSQC spectra of Arc-wt (left) and Arc-MYL (right) at 600 MHz. The assignments of the nitrogen−proton pairs (backbone amide, Arg-NH, and Gln/Asn-NH_2 side chain groups) are denoted. Asterisks denote the Nϵ−Hϵ resonances of arginines that are folded (once) in the ^{15}N dimension, and horizontal lines connect the amino protons of glutamine and asparagine residues. Note that as a consequence of the mutations, the Arg 31 and Arg 40 Nϵ−Hϵ signals are missing in the spectrum of the MYL mutant. The resonances that exhibit large differences in chemical shift upon amino acid substitution are depicted in red in both spectra.

as $\eta - 1$, where η denotes the nuclear Overhauser enhancement.

Structure Determination and Analysis. For the structure determination of Arc-MYL, distance restraints were obtained from NOESY and 3D NOESY-(^{1}H,^{15}N)-HSQC spectra with a mixing time of 100 ms, recorded at 30 °C. Using secondary structure elements for calibration, peak intensities were converted into distances by the r^{-6} relation. The distances were increased by 10% to compensate for spin diffusion. Pseudoatom corrections were added to the upper distance restraint limit for both the methylene and aromatic groups, according to the method of Wüthrich (*22*), while 0.3 Å was added for the methyl groups (*23*). All lower distance restraint limits were set to 1.8 Å. Hydrogen bonds were implemented by using an upper limit distance restraint of 2.3 Å between the corresponding carbonyl oxygen and amide proton and a restraint of 3.3 Å between the carboxyl oxygen and amide nitrogen.

From random coordinates, structures were generated with a simulated annealing protocol using a consistent valence force field (Cvff) with the program Discover (Molecular Simulations Inc.). From this ensemble of structures, a selection was made, on the basis of low total energy and a low number of NOE violations. The final structures were analyzed using InsightII (Molecular Simulations Inc.) and PROCHECK (*24*). The coordinates of the ensemble of structures as well as the NMR restraints have been deposited in the Protein Data Bank under file name 1b28 and r1b28mr, respectively. Additional structure calculations were performed using distance restraints obtained from 2D NOE spectra (τ_{mix} = 100 ms) at 20 and 50 °C, respectively.

RESULTS

Arc-MYL NMR Assignments. The assignments of the NMR resonances of Arc-wt (*11*, *25*) were used as a basis for the assignments of the resonances of the Arc-MYL mutant. A virtually complete assignment was obtained using TOCSY and 3D TOCSY-(^{1}H,^{15}N)-HSQC spectra for spin system analysis and a 3D NOESY-(^{1}H,^{15}N)-HSQC spectrum for sequential analysis. Figure 2 shows the assigned (^{1}H,^{15}N)-HSQC spectrum of Arc-MYL as well as that of Arc-wt. Evidently, several large changes of the chemical shifts of the nitrogen and nitrogen-attached proton resonances occur upon mutation of residues 31, 36, and 40 in the core of the protein. The largest differences between the nitrogen and proton backbone chemical shifts of the wild-type Arc repressor and the MYL mutant are observed for residues 13, 26, 27, 29, 31, 32, 35, 36, 38−42, 45, 46, and 48. Except for residues 13, 46, and 48, the backbone protons of all these residues can be found in close vicinity, i.e., <6 Å, of the mutated side chains. It will be shown that other structural differences in the β-sheet and C-terminus of Arc-wt and Arc-MYL exist that can account for the large difference in the chemical shift for residues 13, 46, and 48.

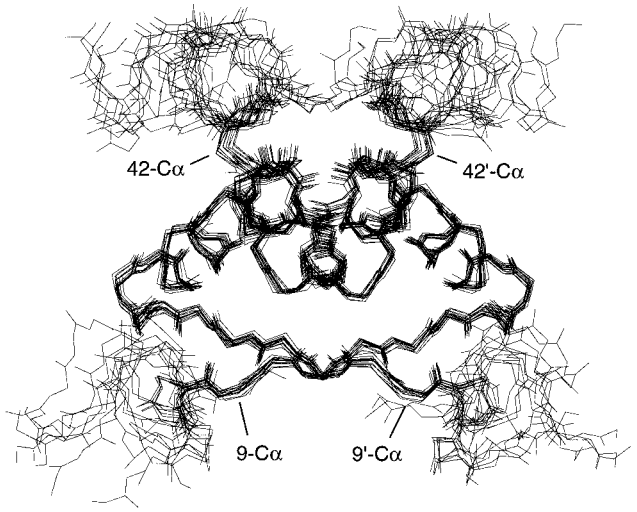

FIGURE 3: Backbone superposition (residues 9−43) of the ensemble of 14 calculated structures of Arc-MYL with a rmsd from the average of 0.37 Å. Note that the second helix appears to be present still beyond residue 43, but is far more disordered than the rest of the backbone of the core.

Arc-MYL Solution Structure. For Arc-MYL, a total of 1722 NOEs per dimer were collected, 1566 of which were intramonomeric and 156 intermonomeric. For the dimeric protein, the intra- and intermonomeric NOEs were distinguished by exploiting the similarity between the structures of Arc-MYL and Arc-wt (*3*). In addition to the NOE distance restraints, 54 hydrogen bonds were used for the regions with a well-defined secondary structure based upon hydrogen−deuterium exchange data (see below). Using a simulated annealing protocol, 40 structures were generated, 14 of which were selected on the basis of low total energy and the absence of NOE violations of >0.5 Å. Figure 3 depicts the backbone superposition of the final ensemble. The refined structures have a very well-defined core region (residues 9−43) with a rmsd from the average of 0.37 ± 0.07 Å for the backbone atoms and 0.83 ± 0.06 Å for all heavy atoms. The high disorder observed for residues 1−8 and 44−52 is due to high mobility as demonstrated by backbone ^{15}N relaxation data (see below). In the Ramachandran plot for the well-defined region, 95.5% of the non-glycine and non-proline residues were found in the most-favored regions, 4.5% in the additionally allowed regions, and none in the disallowed or generously allowed regions.

As compared to that of the NMR structure of the wild-type Arc repressor (*3*), an average rmsd of 0.88 Å for the backbone atoms and an average rmsd of 0.93 Å for all atoms

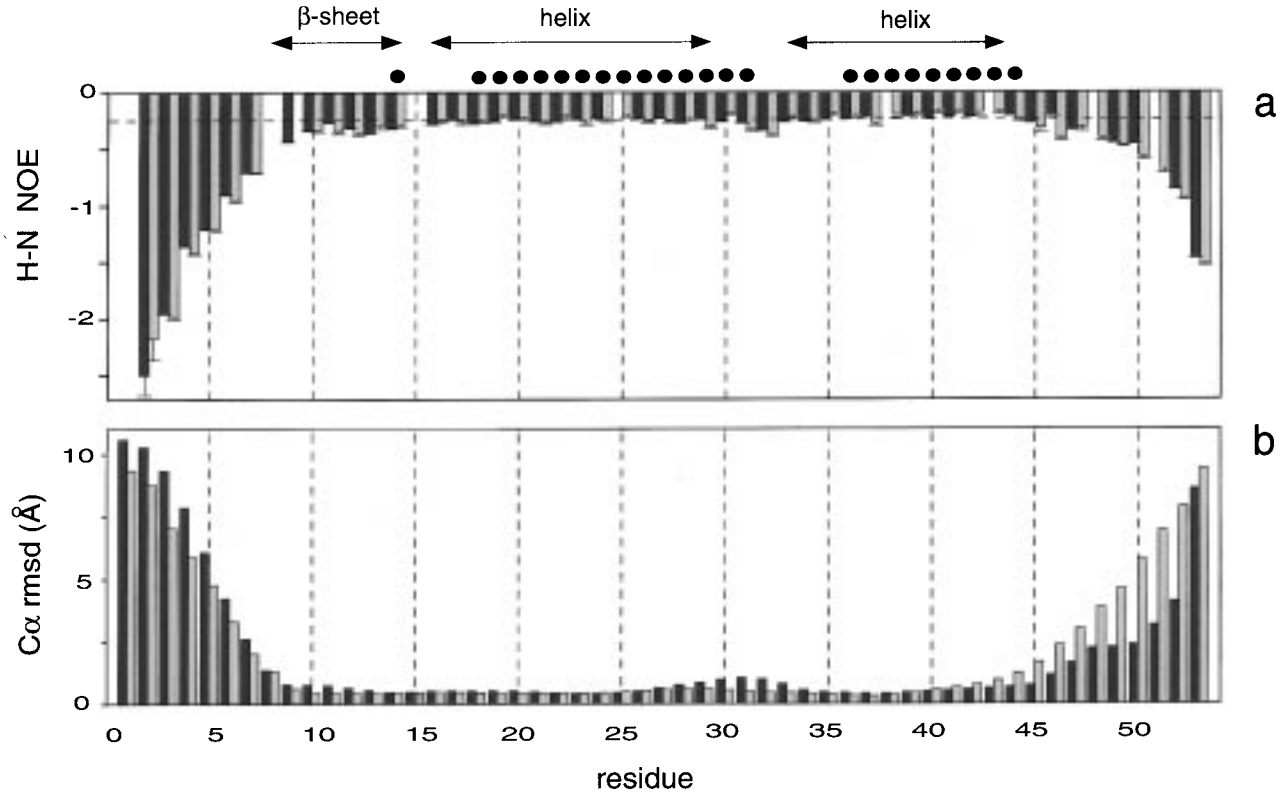

FIGURE 4: Histograms showing (a) the backbone $\{^1H\}-^{15}N$ NOE of Arc-wt (dark gray bars) and Arc-MYL (light gray bars), where the horizontal dashed line denotes the average NOE of the core of the Arc-MYL protein (residues 9−43) at −0.24 to clearly point out the residues that experience increased flexibility, and (b) the rmsd of the backbone atoms in the ensemble of calculated structures of Arc-wt (dark gray bars) and Arc-MYL (light gray bars). The amide protons that showed hydrogen−deuterium exchange rates that were slower than 1×10^{-3} s^{-1} at a protein concentration of 2.6 mM and at pH 4.5 and 30 °C are denoted by black circles at the top of the figure.

(residues 9−43) were found. In solution, the wild-type Arc repressor and the MYL mutant have essentially the same tertiary structure, similar to what has been observed by crystallography (*9*). The packing of the hydrophobic side chains of Met 31, Tyr 36, and Leu 40 in the NMR structure of the MYL mutant resembles the one in the Arc-MYL crystal structure. A detailed comparison of the Arc-MYL and Arc-wt NMR structures, however, reveals a few important differences. The secondary structure elements as defined by Kabsch and Sander (*26*) differ for the second helix; in the wild-type Arc repressor, the second helix runs from residues 34 to 46, whereas in MYL, it starts at residue 33 and ends at residue 43/44 (Figure 3). These results are supported by ^{15}N relaxation and amide hydrogen−deuterium exchange data (see below). The shorter second helix in the MYL mutant can explain the significant differences between Arc-MYL and Arc-wt in the chemical shifts of the backbone nitrogens and protons of residues 46 and 48.

Comparing the orientation of the side chain of Phe 10 and its environment in the solution structure of the MYL mutant with that in other Arc structures, we found that, similar to the crystal structure, in all calculated Arc-MYL solution structures this side chain points toward the solvent and the β-sheet backbone is slightly moved outward. This contrasts with the Arc-wt structures, which all have the "in" conformation. Temperature dependence studies show that the two distinct states interconvert, where the MYL mutant has a stronger tendency toward the "out" conformation (see below).

Backbone Dynamics. Amide hydrogen exchange rates of the MYL mutant were similar to those obtained previously for the wild-type Arc repressor (*25*). Only the α-helical regions and Trp 14 of the β-sheet exhibited exchange rates that were slower than approximately 10^{-3} s^{-1} (Figure 4). In contrast to that in Arc-wt, slow exchange was not observed for the amide proton of Phe 45 at the end of the second helix in Arc-MYL. This suggests that it is not involved in a stable hydrogen bond within the helix structure and confirms the structural results that revealed a shortened second helix in the MYL mutant.

Heteronuclear $\{^1H\}-^{15}N$ NOE of the backbone amides of both Arc-MYL and Arc-wt also yields very similar results (Figure 4a). Low backbone mobility is observed for the core of both proteins (residues 9−43), confirming the close packing of the β-sheet and α-helices. The relaxation data reveal a good correlation with the backbone rmsd of the calculated ensemble of Arc-MYL structures presented here and the Arc-wt ensemble published by Bonvin et al. (*27*) (Figure 4b). The structural disorder that was observed for parts of the NMR structures of both Arc-wt and Arc-MYL can be ascribed to high backbone flexibility. Increased backbone mobility as manifested in $\{^1H\}-^{15}N$ NOEs below the average value of −0.24 (residues 9−43) for both the Arc-MYL and Arc-wt protein is observed for several regions. For the C-terminus, the increased flexibility of the backbone is more pronounced in Arc-MYL than in Arc-wt. This is in agreement with the backbone rmsd in the structural ensembles and the amide hydrogen exchange data. Correspondingly, in contrast to those of Arc-wt, C-terminal residues 52 and 53 were highly disordered in the crystal structure of Arc-MYL (*9*). The loop between the two helices shows a slightly increased flexibility, in line with an increase in the backbone rmsd of the ensemble of structures of both Arc-MYL and

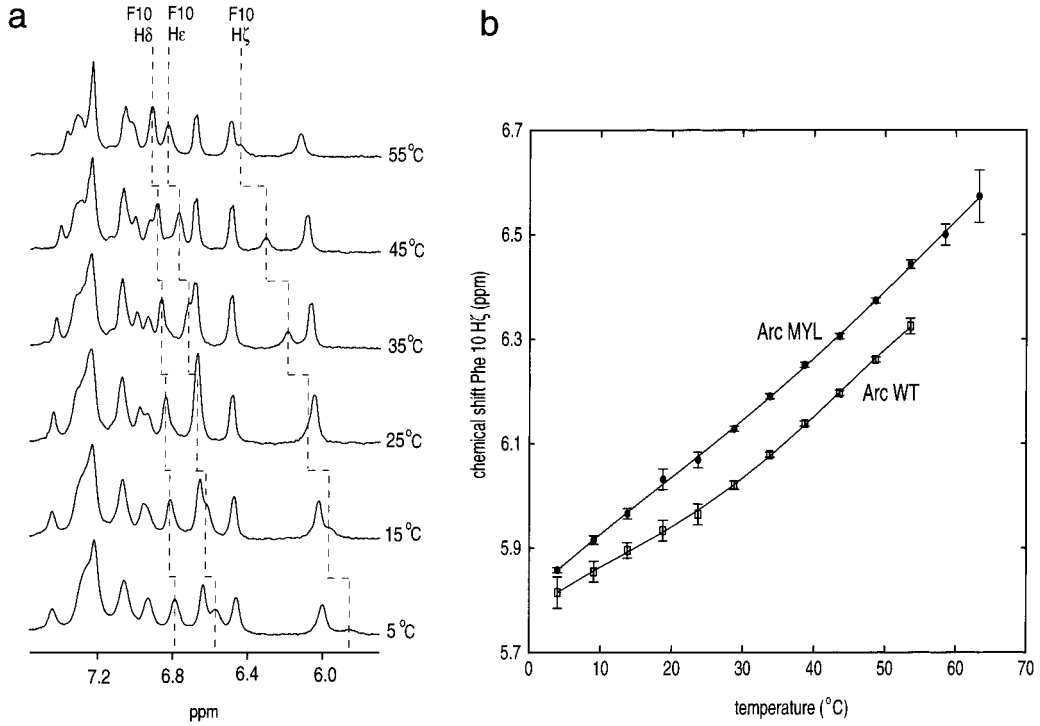

FIGURE 5: (a) Aromatic region of the ^{1}H spectrum of Arc-MYL at 1.0 mM and pD 5.0 in D_2O at different temperatures. The assignments of the Phe 10 aromatic residues are denoted. (b) Temperature dependence of the chemical shift of the Hζ proton of Phe 10 of Arc-wt (□) and Arc-MYL (●) under the same conditions. The error bars represent the uncertainties in the chemical shift reading that is higher in case of overlap (see panel a) or line broadening due to chemical exchange. Similar changes in chemical shift are observed upon addition of urea (see the text and Figure 6).

Arc-wt. Residues Asn 29 and Arg 31 which are situated in this region are involved in cooperative contacts between two Arc dimers upon DNA binding (*4*, *28*). The heteronuclear NOE data of both Arc-MYL and Arc-wt also show increased flexibility for residues that are directly involved in direct DNA contacts. N-Terminal residues 1−7 that interact with the DNA phosphates in the complex are highly mobile for the free protein. Also, residues 9−14 in the recognition β-sheet have significantly increased flexibility as compared to the core of the protein. The relatively high deuterium exchange rates of the amides in the antiparallel β-sheet are consistent with this observation.

Temperature Dependence of Phe 10 Chemical Shifts. The MYL mutant of Arc exhibits a temperature dependence for the chemical shifts of the aromatic protons of Phe 10 similar to that observed previously for Arc-wt (*10*). Figure 5a depicts the aromatic region of the 1D proton spectrum of Arc-MYL at different temperatures that do not exceed melting conditions. A strong temperature dependence of the position of the Phe 10 resonances can be observed with chemical shift changes of up to 0.2 and 0.7 ppm for the Hϵ and Hζ protons, respectively, as measured over the interval from 5 to 60 °C. In addition to the Phe 10 aromatic signals, other signals in the 1D (^{1}H)- and (^{1}H,^{15}N)-HSQC spectra of Arc-MYL that changed their chemical shifts with temperature could all be assigned to atoms in the vicinity near the Phe 10 side chain. This indicates the presence of a temperature-dependent conformational change involving the Phe 10 aromatic ring. Figure 5b shows the Hζ proton chemical shift of both Arc-MYL and Arc-wt as a function of temperature (Figure 5b). Note that due to the relatively higher stability and therefore the increased melting temperature, the Phe 10 resonances of the MYL mutant can be followed up to higher temperatures as compared to Arc-wt before global unfolding sets in. For both proteins, high temperature causes downfield shifts for the resonances of Phe 10, but a significant offset of 0.05−0.11 ppm occurs between the Hζ chemical shifts of Arc-wt and Arc-MYL at 5−55 °C, indicating different behaviors of the temperature-dependent conformational changes. Finally, the observation of a single signal for the Phe 10 Hζ proton in all 1D spectra (Figure 5a) implies that the conformational transition is fast on the NMR time scale (i.e., faster than 2×10^3 s^{-1} under all conditions, based on a 0.7 ppm chemical shift difference).

Urea Dependence of Chemical Shifts. Similar to the thermally induced chemical shift changes (Figure 5), up to about 3 M urea only significant changes are observed in the 1D ^{1}H NMR spectrum of Arc-MYL for the Phe 10 aromatic signals and some resonances of protons close to the Phe 10 ring (Figure 6). These include the methyl groups of Leu 12 and 19, which are visible as the upfield isolated signals in the 1D ^{1}H spectrum. When higher urea concentrations are reached, global unfolding is initiated as a second transition. All transitions were found to be fully reversible. The kinetics of the second transition are slower than those of the premelting transition since the spectra show intermediate exchange on the NMR time scale as demonstrated by the broadened signals measured between 3 and 8 M urea (Figure 6). As the urea concentration approaches 8 M, the 1D ^{1}H spectrum exhibits chemical shifts typical of a denatured protein (see, for example, the methyl proton signal around 1 ppm). These results are in agreement with independent equilibrium unfolding studies of Arc-MYL using optical spectroscopy, showing the disruption of secondary and tertiary structure above 3 M urea (*9*). For Arc-wt, similar results for the urea-dependent changes in chemical shifts of

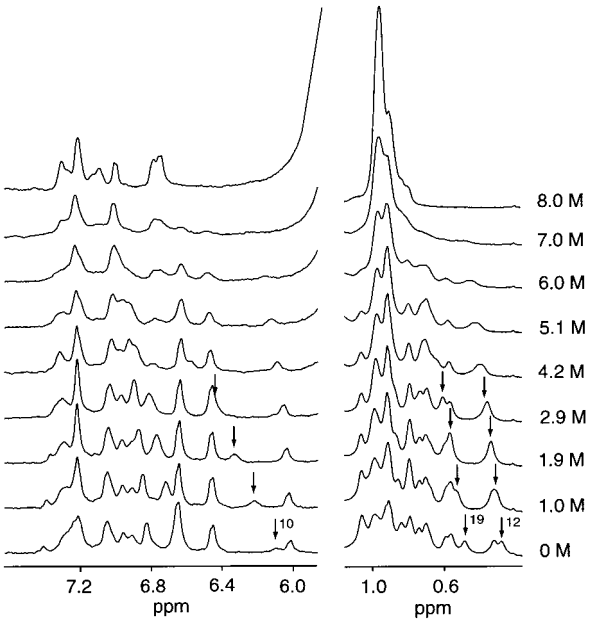

FIGURE 6: Aromatic and methyl region of the 1D ^{1}H spectrum of Arc-MYL (0.5 mM and pH 4.6) in H_2O in the presence of various concentrations of urea (0−8 M). The indicated assignments correspond to the Hζ proton of Phe 10 and the protons of one methyl group of Leu 12 and Leu 19, respectively.

Phe 10 were obtained. Consistent with optical studies that show faster folding kinetics for the MYL mutant than for Arc-wt, the global unfolding transition is in slow chemical exchange on the NMR time scale for Arc-wt.

Temperature Dependence of NOEs Involving Phe 10. Structural insight into the premelting conformational changes due to temperature or urea was obtained by analyzing the NOEs of the Phe 10 ring and its environment under different thermal conditions. NOESY experiments were performed at 20 and 50 °C with a mixing time of 100 ms to characterize two extreme states in the conformational transition as judged from Figure 5b. Below 20 °C, the NOE analysis would be hampered by severe broadening of the NMR signals. Panels a and b of Figure 7 show part of the 2D NOE spectra at 20 and 50 °C, respectively, demonstrating the difference in NOE patterns of the Phe 10 aromatic ring protons at these two temperatures. Most of the long-range NOEs that involve Phe 10 or residues in its vicinity could be unambiguously assigned. The NOEs with Leu 12 could be assigned to either intra- or intermonomeric NOEs after initial modeling using unambiguously assigned NOEs. While at 20 °C NOEs could be identified between the Phe 10 Hϵ ring proton and the Hβ methylene protons of Trp 14′ (the prime indicates the residue from the other monomer), these NOEs vanish at 50 °C. At low temperatures, strong NOEs can be observed between the protons of the aromatic ring of Phe 10 and those of both methyl groups of Leu 19′. These NOEs significantly decrease in intensity at 50 °C. Furthermore, at 50 °C, the Hϵ and Hζ protons exhibit NOEs to one of the methyl groups of Val 33′ that are weak or missing at lower temperatures. The difference in the intensity of the NOE cross-peaks to Leu 12 or Leu 12′ at both temperatures is also consistent with a difference in the conformation under both conditions. A large increase in the NOEs between the Trp 14 Hϵ1, Hζ2, and Hη2 protons and the Hγ and methyl protons of Leu 12 is observed between the 20 and 50 °C NOE spectra, respectively.

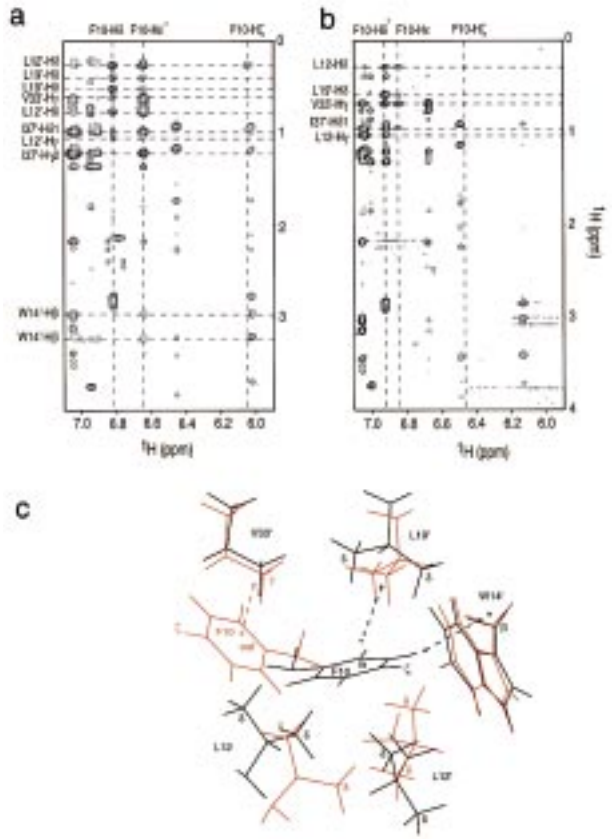

FIGURE 7: Long-range NOE interactions of the Phe 10 aromatic protons in Arc-MYL. Panels a and b show a part of the NOESY spectra in H_2O at 20 (a) and 50 °C (b) demonstrating the different interproton distances. The assignments of the long-range NOEs of the Phe 10 aromatic protons are denoted in both spectra. The asterisks denote overlap: at 20 °C between the Phe 10 Hϵ and the Tyr 36 Hδ protons and at 50 °C between the Phe 10 Hδ and Phe 45 Hζ protons. Note that at higher temperatures the signals are sharper than at lower temperatures. Panel c depicts the spacial environment of the Phe 10 side chain in the "in" (black) and "out" conformations (red). The significant altered NOEs that were found at 20 and 50 °C are denoted by arrows. The coordinates for the "in" and "out" conformations are taken from the NMR structure of Arc-wt and the crystal structure of the Arc-wt−DNA complex, respectively.

On the basis of chemical shift data, no significant structural changes appear to take place from 20 to 50 °C other than those involving or near Phe 10. Hence, a second set of calculations was set up where all long-range NOE distance restraints excluding those involving the side chain protons of Phe 10 and residues in its environment were taken from the complete NOE restraint list at 30 °C. For Phe 10, per dimer, 28 long-range distance restraints in the 30 °C restraint list were removed and two restraint lists corresponding to the low- and high-temperature conformations were generated by adding 46 and 26 restraints, respectively. Additionally, per dimer 12 NOE distance restraints between Leu 12 and Trp 14 in the 30 °C restraint list were substituted by 14 different distance restraints for the 20 and 50 °C temperature set. With both the 20 and 50 °C sets of restraints, an ensemble of 20 structures was generated, applying the same protocol that was used for the structure calculations described above.

For the low-temperature case, all 20 calculated structures of Arc-MYL revealed the aromatic ring packed in the core of the protein. The χ_1 dihedral angle was identified as gauche$^-$ (60°), characteristic of the Phe 10 "in" conformation.

In contrast, throughout the whole ensemble of structures, the conformational state of Phe 10 at 50 °C shows a χ_1 dihedral angle corresponding to a trans rotameric state, or "out" conformation. Intraresidual NOEs and *J*-coupling constants between the Phe 10 NH and β-methylene protons that also provide information about the rotameric state of the χ_1 torsion angle are in agreement with these results. At 20 °C, the *J*-coupling data are consistent with a preferred gauche rotameric state for the χ_1 torsion angle, whereas at 50 °C, the data suggest an increased population of the trans rotameric state. In addition to the χ_1 rotameric state of Phe 10, the position of the Leu 12 side chain differs significantly between the structures at low and high temperatures. When the Phe 10 ring is directed outward, the side chain of Leu 12′ partly occupies the area that is left by the Phe 10 ring by packing against Trp 14′ that initially interacted with Phe 10.

The conformations at low and high temperatures resemble the distinct Phe 10 "in" and "out" conformations as they appear in the free wild-type Arc repressor and the Arc−DNA complex structure, respectively (Figure 7c). Most crucial short distances for both conformations could be identified as unambiguous NOEs in the spectra of Arc-MYL at low and high temperatures and are denoted in Figure 7c. The Phe 10 "in" conformation allows interactions of the Phe 10 ring with residues in the core of the molecule, such as Leu 12′, Trp 14′, and Leu 19′. The extended Phe 10 "out" conformation lacks close contacts to Trp 14′ but appears to be close to Leu 12 and Val 33′.

DISCUSSION

These studies describe a premelting transition of the Arc repressor in structural terms. It is shown that it mainly entails a conformational change at Phe 10 and repacking of the hydrophobic core. The existence of native-like dimeric folding intermediates was previously suggested from the urea and viscosity dependence of refolding kinetics of Arc (*13*, *14*). In more recent optical studies, the premelting transition could be monitored by a red shift of fluorescence emission upon increasing the urea concentration up to 3 M for Arc-wt and several Arc mutants (C. Robinson, personal communication). This change in fluorescence is consistent with a change in the environment of the single tryptophan, Trp 14, upon displacement of the Phe 10 side chain (Figure 7c). By fluorescence, no premelting transition was observed for the FV10 mutant, which confirms the key role of Phe 10 in the transition. Next to the displacement of the Phe 10 ring, the premelting transition likely also involves small structural adjustments of the β-sheet (Figure 1c) that may destabilize the backbone to backbone intermonomeric hydrogen bonds. This may contribute to the relatively fast exchange observed for the amide protons of the β-sheet in both Arc-wt (*25*) and Arc-MYL as compared to that of the amides of the helical regions.

Both the hydrogen−deuterium exchange and $\{^1H\}-^{15}N$ NOE data support the instability of the antiparallel β-sheet that forms between residues 8 and 14 of each monomer. This flexibility in the backbone of the DNA binding β-sheet allows the structure to adapt during the DNA binding process and might help position the side chains of residues 9, 11, and 13 to make the direct DNA base contacts (*4*). The largest main chain movements in the β-sheet are detected for Leu 12. The backbone carbonyl of Leu 12′ is involved in an intermonomeric hydrogen bond to the backbone amide proton of Phe 10 whose side chain is involved in the equilibrium between the "in" and "out" conformations. In addition, the side chain of Leu 12 is involved in the structural reorientation of the core domain associated with the change in the rotameric state of the Phe 10 side chain. Phe 10 as well as the amino terminal residues is involved in a large number of important phosphate backbone contacts with the operator DNA (*4*, *5*), and they all contribute to the specificity of the recognition process as determined by mutagenesis studies (*6*, *29*). The mixture of interconverting states at Phe 10 and the highly dynamical properties of the N-terminal residues as well as the increased flexibility of the β-sheet can provide the repressor with a mechanism for exploring the DNA sequence of its operator more efficiently for finding the specific complementary fit.

The aromatic proton chemical shifts of Phe 10 can be used as a monitor of the equilibrium involving the side chain orientation in Arc-wt and Arc mutants (Figure 5b), provided that no other structural changes relative to Arc-wt occur that can influence the chemical shifts of Phe 10. It can be assumed that the mutated side chains in MYL do not directly affect the Phe 10 chemical shifts. Therefore, the significant downfield shift of the Hζ resonance in Arc-MYL as compared to Arc-wt reflects a relatively higher population of the Phe 10 "out" conformation in Arc-MYL. The difference in the preference of either of the Phe 10 conformations is also apparent in the crystal structures of Arc-MYL and Arc-wt, where the most favorable conformation is frozen in the crystal lattice. The substantially altered folding properties as revealed in optical studies were suggested to involve a lowering of the energetic barrier of the transition between the partially folded dimer and the native dimer in Arc-MYL (*12*−*14*) and may explain these results.

The correlation between the chemical shifts of the Phe 10 aromatic protons of Arc and the equilibrium state of the position of the side chain can be applied to the Arc-PL8 mutant as well. This mutant forms an antiparallel β-sheet extended by two additional hydrogen bonds, which are introduced by substitution of Pro 8 with a leucine (*8*). The highly upfield shifted resonances of the Phe 10 aromatic protons in PL8 (*30*) can be used to predict that the equilibrium between the two distinct Phe 10 side chain conformations is largely shifted to the "in" conformation. Indeed, in the crystal structure of the PL8 mutant, the Phe 10 side chain has a clear "in" conformation (*8*). Furthermore, the lack of temperature dependence of the Phe 10 chemical shifts suggests that in the PL8 mutant the transition that reorients the Phe 10 side chain does not occur. The significantly decreased specific DNA binding affinity of Arc-PL8 (by a factor of 200) was previously attributed to the extended β-sheet that hinders the N-terminal residues to adopt the right conformation (*6*, *8*). However, the absence of the premelting transition that directs the Phe 10 conformation outward may be the main cause of the lower DNA binding affinity and the loss of specificity. This emphasizes the importance of the ability to orientate the Phe 10 ring and of the flexibility of the DNA-binding site that is likely also more restricted in the PL8 mutant.

In summary, the results as described in this paper provide a clear picture of dynamical behavior on the nano- to

millisecond time scale of the Arc repressor in solution. The two distinct conformations that can be identified in the three-dimensional structures of free wild-type Arc repressor and the Arc−DNA complex (Figure 1) coexist and readily exchange. At and below room temperature, the "in" conformation is more stable than the "out" conformation both in Arc-wt and in Arc-MYL. The "in" conformation is, however, not the functionally active state of the Arc dimer. In the less stable but functionally active form, the aromatic ring of Phe 10 is exposed to the solvent and the burial of the apolar surface of the side chain of Phe 10 may have significant implications in the thermodynamics of the DNA binding process. A high population of the functionally active dimeric state of the unbound Arc can be induced by DNA binding as well as by high temperatures and by urea. The conformational changes that accompany the premelting transition and main chain mobility in the DNA binding site can speed the target DNA recognition and provide the mechanism for induced fit binding of the Arc repressor.

ACKNOWLEDGMENT

We thank Ingrid Luyten for carrying out initial relaxation measurements on the wild-type Arc repressor. We also thank Cliff Robinson for helpful discussions and C. Kissinger and C. O. Pabo for making available the coordinates of the 1.8 Å resolution crystal structure of the wild-type Arc repressor.

REFERENCES

1. Susskind, M. M., and Youderian, P. (1983) in *Lambda II* (Hendrix, R. W., Roberts, J. W., Stahl, F. W., and Weisberg, R., Eds.) pp 347−366, Cold Spring Harbor Laboratory Press, Cold Spring Harbor, NY.
2. Vershon, A. K., Youderain, P., Susskind, M. M., and Sauer, R. T. (1985) *J. Biol. Chem. 260*, 12124−12129.
3. Breg, J. N., van Opheusden, J. H. J., Burgering, M. J. M., Boelens, R., and Kaptein, R. (1990) *Nature 346*, 586−589.
4. Raumann, B. E., Rould, M. A., Pabo, C. O., and Sauer, R. T. (1994) *Nature 367*, 754−757.
5. Raumann, B. E., Brown, B. M., and Sauer, R. T. (1994) *Curr. Opin. Struct. Biol. 4*, 36−43.
6. Vershon, A. K., Bowie, J. U., Karplus, T. M., and Sauer, R. T. (1986) *Proteins: Struct., Funct., Genet. 1*, 302−311.
7. Knight, K. L., and Sauer, R. T. (1989) *Proc. Natl. Acad. Sci. U.S.A. 86*, 797−801.
8. Schildbach, J. F., Milla, M. E., Jeffrey, P. D., Raumann, B. E., and Sauer, R. T. (1995) *Biochemistry 34*, 1405−1412.
9. Waldburger, C. D., Schildbach, J. F., and Sauer, R. T. (1995) *Nat. Struct. Biol. 2*, 122−128.
10. Breg, J. N., Boelens, R., George, A. V. E., and Kaptein, R. (1989) *Biochemistry 28*, 9826−9833.
11. Bowie, J. U., and Sauer, R. T. (1989) *Biochemistry 28*, 7139−7143.
12. Robinson, C. R., Rentzeperis, D., Silva, J. L., and Sauer, R. T. (1997) *J. Mol. Biol. 273*, 692−700.
13. Waldburger, C. D., Jonsson, T., and Sauer, R. T. (1996) *Proc. Natl. Acad. Sci. U.S.A. 93*, 2629−2634.
14. Jonsson, T., Waldburger, C. D., and Sauer, R. T. (1996) *Biochemistry 35*, 4795−4802.
15. Griesinger, C., Otting, G., Wüthrich, K., and Ernst, R. R. (1988) *J. Am. Chem. Soc. 110*, 7870−7872.
16. Jeener, J., Meier, B. H., Bachmann, P., and Ernst, R. R. (1979) *J. Chem. Phys. 71*, 4546−4553.
17. Bothner-By, A. A., Stephens, R. L., Lee, J., Warren, C. D., and Jean-loz, R. W. (1984) *J. Am. Chem. Soc. 106*, 811−813.
18. Cavanagh, J., Fairbrother, W. J., Palmer, A. G., III, and Skelton, N. J. (1996) in *Protein NMR Spectroscopy, principles and practice*, Academic Press, New York.
19. Dayie, K. T., and Wagner, G. (1994) *J. Magn. Reson., Ser. A 111*, 121−126.
20. Vis, H., Vorgias, C. E., Wilson, K. S., Kaptein, R., and Boelens, R. (1998) *J. Biomol. NMR 11*, 265−277.
21. Delaglio, F., Grzesiek, S., Vuister, G. W., Zhu, G., Pfeifer, J., and Bax, A. (1995) *J. Biomol. NMR 6*, 277−293.
22. Wüthrich, K. (1986) in *NMR of Proteins and Nucleic Acids*, Wiley, New York.
23. Koning, T. G. M., Boelens, R., and Kaptein, R. (1990) *J. Magn. Reson. 90*, 111−123.
24. Laskowski, R. A., MacArthur, M. W., Moss, D. S., and Thornton, J. M. (1993) *J. Appl. Crystallogr. 26*, 283−291.
25. Burgering, M. J. M., Hald, M., Breg, J. N., Boelens, R., and Kaptein, R. (1995) *Biopolymers 35*, 217−226.
26. Kabsch, W., and Sander, C. (1983) *Biopolymers 22*, 2577−2637.
27. Bonvin, A. M. J. J., Vis, H., Breg, J. N., Burgering, M. J. M., Boelens, R., and Kaptein, R. (1994) *J. Mol. Biol. 236*, 328−341.
28. Brown, B. M., Bowie, J. U., and Sauer, R. T. (1990) *Biochemistry 29*, 11189−11195.
29. Brown, B. M., Milla, M. E., Smith, T. L., and Sauer, R. T. (1994) *Nat. Struct. Biol. 1*, 164−168.
30. Zagorski, M. G., Bowie, J. U., Vershon, A. K., Sauer, R. T., and Patel, D. J. (1989) *Biochemistry 28*, 9813−9825.

BI982677T